

Durham Research Online

Deposited in DRO:

25 July 2016

Version of attached file:

Accepted Version

Peer-review status of attached file:

Peer-reviewed

Citation for published item:

Burton-Johnson, A. and Macpherson, C. and Hall, R. (2017) 'Internal structure and emplacement mechanism of composite plutons : evidence from Mt Kinabalu, Borneo.', *Journal of the Geological Society.*, 174 (1). pp. 180-191.

Further information on publisher's website:

<https://doi.org/10.1144/jgs2016-041>

Publisher's copyright statement:

Journal of the Geological Society First published online September 22, 2016 <https://doi.org/10.1144/jgs2016-041> © Geological Society of London 2016.

Use policy

The full-text may be used and/or reproduced, and given to third parties in any format or medium, without prior permission or charge, for personal research or study, educational, or not-for-profit purposes provided that:

- a full bibliographic reference is made to the original source
- a [link](#) is made to the metadata record in DRO
- the full-text is not changed in any way

The full-text must not be sold in any format or medium without the formal permission of the copyright holders.

Please consult the [full DRO policy](#) for further details.

1 **Internal structure and emplacement mechanism of composite plutons: Evidence from**
2 **Mt Kinabalu, Borneo**

3 Alex Burton-Johnson*¹; Colin G. Macpherson² & Robert Hall³

4 ¹British Antarctic Survey, High Cross, Madingley Road, Cambridge, CB3 0ET, UK

5 *Corresponding author (e-mail: alerto@bas.ac.uk)

6 ²Department of Earth Sciences, University of Durham, Durham, DH1 3LE, UK

7 ³SE Asia Research Group, Department of Geology, Royal Holloway, University of London,
8 Egham, Surrey TW20 0EX, UK

9

10 *Word count*

11 Abstract and body: 5,649

12 Table and figure captions: 757

13 References: 1,790

14 *Number of Figures*

15 12

16 *Keywords*

17 Mt Kinabalu, SE Asia, emplacement, tectonics, intrusion, pluton, granite, granodiorite

18 **Abstract**

19 The internal structure and emplacement mechanisms of composite plutons are
20 investigated using new field data from the composite Late Miocene granitic intrusion of
21 Mt Kinabalu in northern Borneo. The pluton was emplaced in the upper to middle crust
22 in the Late Miocene at the contact between the ultramafic basement and sedimentary
23 cover rocks. Structural data indicates that emplacement occurred during regional NNW-
24 SSE oriented extension, challenging tectonic models that infer contemporaneous
25 regional compression. The six major units comprising the pluton were accommodated by
26 upward flexure of the cover rocks with most magma pulses emplaced successively
27 beneath their predecessors. However, the irregular three-dimensional internal structure
28 of the pluton also reflects preferential emplacement of successive units along the
29 granite-country rock contact of previous units in preference to the basement-cover rock
30 contact exploited by the initial units. This work highlights the complex emplacement
31 mechanisms and internal structure of composite intrusions and assesses how they differ
32 from models of tabular emplacement.

33

34 **Introduction**

35 Interpretations of ascent and emplacement of granitic intrusions have changed
36 drastically in recent decades from models of large diapirs ascending slowly through the
37 crust to models of rapid dyke-fed ascent and layered, laccolith-style emplacement of
38 composite plutons (Clemens & Mawer 1992, Petford *et al.* 2000, Petford & Clemens
39 2000, McCaffrey & Petford 1997, Cruden 1998, Cruden & McCaffrey 2001, Grocott *et al.*
40 2009, Vigneresse & Clemens 2000, Horsman *et al.* 2009, de Silva & Gosnold 2007, de
41 Saint-Blanquat *et al.* 2001, de Saint-Blanquat *et al.* 2006, Vigneresse 2006, Wiebe &
42 Collins 1998, Wiebe 1988). Mt Kinabalu in Sabah, NW Borneo (Fig. 1), is an Upper
43 Miocene intrusion with a 4095 m high glaciated summit and good exposure over a
44 vertical range of 2900m (Fig. 2), providing an excellent opportunity to study the structure
45 of a granitoid pluton in three dimensions. Cottam *et al.* (2010) reinterpreted the intrusion
46 as a composite laccolith formed by discrete magmatic pulses based on geochronological
47 constraints. However, no detailed mapping of the pluton has been undertaken for four
48 decades, largely due to its extreme relief and difficulties in accessing its densely forested
49 flanks. We present the first new map of the pluton since Jacobson (1970) and reinterpret
50 its structure and emplacement, then discuss the implications for global magmatic
51 processes.

52 **Regional geological history and tectonic setting**

53 Northern Borneo has a basement of Mesozoic igneous and metamorphic rocks overlain
54 by Cenozoic sediments. The basement includes mafic igneous rocks and radiolarian
55 cherts, variably serpentinised peridotites and Triassic to Cretaceous rocks previously
56 described as crystalline basement (Reinhard & Wenk 1951, Dhonau & Hutchison 1965,
57 Koopmans 1967, Kirk 1968, Leong 1974). The latter resemble deformed ophiolitic rocks
58 intruded by arc plutonic rocks that Hall & Wilson (2000) suggested formed in a Mesozoic,
59 intra-oceanic arc. The peridotites have been interpreted as part of a Cretaceous ophiolite
60 (Hutchison 2005) emplaced in the Late Cretaceous or Early Paleogene (Newton-Smith
61 1967, Omang & Barber 1996). Unusual peridotites exposed close to Mount Kinabalu have
62 been interpreted to represent sub-continental mantle (Imai & Ozawa 1991). The
63 basement is in contact with a cover sequence of predominantly deep-water turbidites

64 and related deposits assigned to the Eocene to Lower Miocene Trusmadi and Crocker
65 Formations (Collenette 1965, van Hattum *et al.* 2006).

66 The basement and cover rocks were folded and faulted during Eocene and Oligocene
67 deformation that was driven by the subduction of the proto-South China Sea beneath
68 Borneo (Taylor & Hayes 1983; Rangin & Silver 1990; Tongkul 1991, 1994; Hall 1996; Hall
69 & Wilson 2000; Hutchison 2000). The attenuated South China continental margin
70 collided with northern Borneo in the Early Miocene (Hutchison 2000, Hall & Wilson 2000)
71 resulting in the Sabah Orogeny (Hutchison 1996), which produced significant topography
72 in the region (Hutchison 2000) and emergence of much of Sabah and the present central
73 highlands of northern Borneo. However, by the end of the Early Miocene much of
74 present-day Sabah was below or close to sea level (Noad 1998, Balaguru *et al.* 2003, Hall
75 *et al.* 2008), probably with a low elevated range of hills at the position of the Crocker
76 Mountains. Offshore the Neogene shelf edge migrated broadly northwestwards from the
77 Middle Miocene onwards (Sandal 1996, Hazebroek & Tan 1993, Hutchison 2005, Cullen
78 2010), suggesting a gradual rise and widening of the Crocker Mountains during the
79 Middle and Late Miocene. The Kinabalu granite was intruded into the centre of the
80 Crocker Mountains between 8 and 7 Ma (Cottam *et al.* 2010). High post-emplacement
81 exhumation rates indicated by low temperature thermochronology are comparable to
82 the exhumation rates of mountainous terrains (Cottam *et al.* 2013), suggesting that the
83 Crocker Range existed at the time of emplacement.

84 Sabah became fully emergent only at the end of the Miocene or Early Pliocene
85 (Collenette 1965, Balaguru *et al.* 2003, Tongkul & Chang 2003, Morley & Back 2008). The
86 glaciated summit plateaus and Pleistocene glacial tills (Collenette 1958) of the Kinabalu
87 area, and similar deposits near to Mount Tambuyukon, indicate that the summits of
88 Kinabalu, Tambuyukon and possibly Trusmadi, were significantly higher than other parts
89 of the Crocker Range by the Pleistocene.

90 **Results**

91 *New geological maps*

92 A limited number of field studies on the geology of Mt Kinabalu have been published
93 (Reinhard & Wenk 1951, Collenette 1958, Kasama *et al.* 1970, Jacobson 1970). At the
94 time of this previous mapping the mountain was even less accessible than today with
95 more extensive rainforest cover and much poorer transport systems. As such, access was
96 largely restricted to the lowland streams south of the mountain. Our work augments the
97 observations of Jacobson (1970), the most recent detailed study, with new traverses of
98 the intrusion focusing on the previously unmapped high altitude regions including the
99 eastern and northern ridges.

100 A new digital elevation model (DEM) was created during this study based on published
101 topographic maps, a high resolution satellite image (1m resolution) and GPS
102 observations collected during fieldwork. Fig. 3 presents the revised geological map of Mt.
103 Kinabalu. Draping the map over the digital elevation model in Fig. 4 illustrates how the
104 relief is controlled by the surface lithologies. Localities referred to on the summit
105 plateaux are highlighted on the large scale summit map in Fig. 5. Combining the field
106 observations with the chronology of Cottam *et al.* (2010) allows us to infer the internal
107 structure of the pluton (Figs. 6 and 7).

108 **Lithological Units**

109 *Ophiolitic basement*

110 The ophiolitic basement is the oldest lithological unit in Sabah and underlies much of the
111 region (Fig. 1). Outcrops of the ophiolite around Mt Kinabalu are predominantly
112 lherzolite but there is also wehrlite, harzburgite and dunite, with varying degrees of
113 serpentinisation (Jacobson 1970).

114 Fluvial pebbles 11km SE of Mt Kinabalu comprise garnet pyroxenites (in agreement with
115 Imai & Ozawa 1991), amphibolite, garnet amphibolite, garnet-zeolite amphibolite and
116 amphibolite-plagioclase gneiss, amygdale-rich basaltic volcanics and chert. Some of
117 these lithologies are similar to rocks described from the Darvel Bay ophiolite (Leong

118 1974, Hutchison 1978, Omang & Barber 1996) and also resemble the description of Mt
119 Kinabalu's "crystalline basement" (Jacobson 1970).

120 Ultramafic hornfels containing relict olivine and orthopyroxene with secondary chlorite,
121 serpentine and talc is found downstream of the granite-ophiolite contact on the SE of
122 the pluton in the river of S. Bambang (Fig. 3). Some of the ultramafic rocks in contact
123 with the Paka Porphyritic Granite on the summit trail are variably (sometimes
124 intensively) altered to talc, and schists containing varying abundances of tremolite,
125 anthophyllite and talc are described on the south of the mountain by Jacobson (1970).

126 *Crocker Formation turbidite sediments*

127 The interbedded turbiditic mudstones and quartzarenite to subarkose sandstones of the
128 Crocker Formation overlie the ophiolitic basement. The contact was not observed on the
129 north of the mountain but a metamorphic aureole of sandstones metamorphosed to
130 quartzite extends ~20m to 2 km from the pluton. The contact between the sediments
131 and granite was observed in S. Tahobang to the west of the intrusion (Fig. 3). For up to 8
132 m from the contact, sedimentary rocks have been metamorphosed to a hornfels of very
133 fine sutured quartz grains, chlorite, minor biotite, and interstitial secondary muscovite.
134 Jacobson (1970) observed contact metamorphism up to 1.6 km from the pluton where a
135 mica-cordierite hornfels close to the contact in S. Kilambuan (west of the mountain, Fig.
136 3) contains biotite, muscovite, cordierite quartz and albite.

137 *The Mt Kinabalu Pluton*

138 The Mt Kinabalu pluton comprises six major units classified by modal mineral
139 abundances determined by point counting of 46 thin sections stained for plagioclase and
140 K-Feldspar (Sperber 2009). Table 1 presents the modal mineralogy of these intrusive
141 units, along with U-Pb ages from zircon rims (Cottam *et al.*, 2010). Estimates of volumes
142 for each unit are included based on the mapped extent (Fig. 3) and the interpreted pre-
143 erosion cross-section of the pluton (Fig. 6). Calculation of these volumes is discussed
144 further in the 'Discussion' section below. Although the modal mineralogy of many of the
145 units are very similar, they can be distinguished in the field (although sometimes only on
146 fresh surfaces) and were mapped according to these mineralogical differences (with the

147 exception of the Low's Granite which was distinguished from the King Granite using
148 mineralogical, chemical and magnetic susceptibility data).

149 Petrographic descriptions and field relationships between the units are given below, with
150 more detailed information in Burton-Johnson (2013). We include two newly recognised
151 units, the King Granite and the Paka Porphyritic Granite. The King Granite was previously
152 mapped as part of the Low's Granite (under the name "Hornblende Granite", Cottam *et al.* 2010) and the Paka Porphyritic Granite was included as part of the Mesilau Porphyritic
153 Granite (previously named the "Porphyritic Hornblende Granite", Cottam *et al.* 2010).
154 The revised classification (Fig. 8) differs from previous work (Reinhard & Wenk 1951, Kirk
155 1968, Vogt & Flower 1989) as summarised in Cottam *et al.* (2010), which partly reflects
156 changing classification schemes, and partly the result of mineral misidentifications in
157 some earlier studies probably due to a lack of thin section mineral staining. Key
158 differences are: (i) that we find more consistent modal mineralogies for each unit in this
159 study than previous mineralogical data suggested; (ii) the Alexandra
160 Tonalite/Granodiorite unit, previously classified as a monzodiorite (Vogt & Flower 1989),
161 ranges from tonalite to granodiorite with varying potassium feldspar content (4-7%); and
162 (iii) that the majority of units are granites, not granodiorites or quartz monzonites.
163

164 *Alexandra Tonalite/Granodiorite*

165 The Alexandra Tonalite/Granodiorite is the oldest unit and forms most of the western
166 summit peaks of the Western Plateau. It is composed of 1-3 mm grains of quartz,
167 plagioclase, K-feldspar, hornblende and biotite crystals. Biotite is the dominant
168 ferromagnesian phase, although biotite pseudomorphs of hornblende indicate that
169 much may be secondary. Secondary biotite occurs in all the granite units but is
170 particularly prevalent in the Alexandra Tonalite/Granodiorite. Foliation of the biotite
171 crystals was observed to dip at ~40-65° towards the south-west.

172 *Low's Granite*

173 The Low's Granite was emplaced below and around the Alexandra
174 Tonalite/Granodiorite, forming the eastern and southern peaks on the Western Plateau
175 and a separate unconnected region on the mountain's northern flank (Fig. 3). The unit is
176 composed of 4-7 mm long euhedral prismatic hornblende phenocrysts (the dominant

177 ferromagnesian phase) in a groundmass of 1-4 mm grains of K-feldspar, plagioclase,
178 hornblende and biotite. Samples from the northern flank contain more K-feldspar and
179 quartz than those of the Western Plateau.

180 The contact of the Alexandra Tonalite/Granodiorite and Low's Granite was observed on
181 the Western Plateau. Along the eastern extent of the Alexandra Tonalite/Granodiorite
182 this contact steepens to vertical and in some places the Low's Granite is found above the
183 Alexandra Tonalite/Granodiorite, enveloping the older unit (Fig. 7 and 9). West of this
184 the contact dip shallows to $\sim 20^\circ$ to the WSW and becomes sub-parallel to the
185 topographic surface, revealing windows of the Low's Granite within the Alexandra
186 Tonalite/Granodiorite (Fig. 9). The contact is sharp when sub-vertical but appears to be
187 more gradational (over 1-3 m) where dipping at a low angle. When sharp, the contact
188 shows chlorite, hematite and epidote mineralisation along the contact surface and the
189 Low's Granite shows a 2 m wide chilled margin of more intense irregular and contact-
190 parallel fracturing, finer crystal sizes, more abundant biotite and extensive chlorite
191 mineralisation of ferromagnesian minerals, grading in to its interior composition (Fig.
192 10a). No chilled margin is expressed in the Alexandra Tonalite/Granodiorite. These field
193 relations support emplacement of the Low's Granite after the Alexandra
194 Tonalite/Granodiorite.

195 *King Granite*

196 The most extensive unit is the King Granite, emplaced beneath the Low's Granite. Crystal
197 sizes and mineralogy are similar to the Low's Granite but with a lower modal abundance
198 of ferromagnesian phases (especially biotite) and a greater amount of K-feldspar. The
199 contact can be observed on the eastern cliff of the Western Plateau (Fig. 10b). This
200 inaccessible outcrop shows a lighter body of King Granite in sharp contact with the
201 overlying, darker Low's Granite. The lighter body darkens gradationally away from the
202 contact, which dips at $\sim 50^\circ$ NW. Dykes of King Granite with sharp contacts intrude the
203 overlying Low's Granite (Fig. 10b) so the periphery of the Low's Granite had solidified
204 during the 0.2 My time gap inferred from zircon geochronology (Cottam *et al.* 2010), and
205 support emplacement of the King Granite after the Low's Granite. Elsewhere the Low's
206 and King Granites are almost identical in the field so the contact location is largely

207 inferred from geochemical and Anisotropic Magnetic Susceptibility (AMS) data (Burton-
208 Johnson 2013).

209 *Donkey Granite*

210 Jacobson (1970) described this unit as a minor biotite adamellite porphyry but our work
211 shows it to be much more extensive than previously mapped, intruding the King Granite
212 on the Western and Eastern Plateaux and in Low's Gully 600 m below (Fig. 5 and 10c).
213 We interpret these three occurrences as a NE-trending, sub-vertical planar sheet,
214 approximately 2.5 km long and 200 m wide. The Donkey Granite is mineralogically similar
215 to the King Granite, composed of hornblende, biotite and ≤ 4 mm long subhedral tabular
216 plagioclase phenocrysts in a finer hornblende, biotite, plagioclase, quartz and K-feldspar
217 groundmass.

218 On the Western Plateau the sub-vertical western and eastern margins of the Donkey
219 Granite are different from each other (Fig. 5). The eastern contact is largely gradational
220 but becomes sharp where it forms the distinctive Donkey's Ears Peak (Fig. 10d). The
221 western contact is sharp along its length with sub-vertical, contact-parallel flow banding
222 within the Donkey Granite and localised magma mingling with the King Granite (Fig. 10e),
223 implying that neither body was solid when the Donkey Granite was intruded.

224 *Paka Porphyritic Granite*

225 The Paka Porphyritic Granite was emplaced after the King Granite (based on contact
226 relations and geochronology) along the southern flank of the pluton. It is found to the
227 south and east of the Eastern Plateau and at lower elevations on the NW flank. The unit
228 contains subhedral, tabular, K-feldspar megacrysts of 10-15 mm length in a groundmass
229 of 2-5 mm long K-feldspar, plagioclase, quartz, hornblende and biotite crystals.
230 Megacrysts commonly show long axis alignment plunging at a low angle ($<26^\circ$) but with
231 varying azimuths, even across a single outcrop.

232 The contact of the King and Paka Porphyritic Granites is sharp and often apparent in the
233 topography as steep cliffs around the Eastern Plateau. Proximal to the King Granite,
234 megacrysts become more abundant in the Paka Porphyritic Granite which also shows
235 contact-parallel flow banding and megacryst alignment (Fig. 10f) implying emplacement

236 of the Paka Porphyritic Granite after the King Granite. Along Mt Kinabalu's southern
237 flanks the contact dips steeply south (67-82° S) with the Paka Porphyritic Granite
238 overlying the older unit, but the orientation changes on the Eastern Plateau where the
239 Paka Porphyritic Granite underlies the King Granite (Fig. 6, 7 and 10g). Hydrothermal
240 channelling proximal to the contact has produced strong haematite alteration of the
241 overlying units, including at the consequently named "Red Rock Peak" on the Eastern
242 Plateau (Fig. 5 and 10g).

243 *Mesilau Porphyritic Granite*

244 The southeast portion of the main pluton is composed of the Mesilau Porphyritic Granite,
245 which also forms the mineralised satellite stock of the disused Mamut porphyry copper
246 mine (Fig. 3). The northern extent of the main mass was not observed but is interpreted
247 from prominent topographic ridges and valleys. Previously mapped as a variant of the
248 Paka Porphyritic Granite, the Mesilau Porphyritic Granite shows clear differences in
249 mineralogy, chemistry and field relations (Burton-Johnson 2013). Most notably the
250 Mesilau Porphyritic Granite possesses large, 20-30 mm long, subhedral, tabular, K-
251 feldspar megacrysts that comprise approximately 30% of the rock and are commonly
252 aligned. The groundmass consists of 3-5 mm long crystals of K-feldspar, plagioclase,
253 quartz, hornblende and biotite and ≤2% clinopyroxene.

254 We could not locate contacts of the Mesilau Porphyritic Granite with other units. These
255 were inferred from changes in float on opposite sides of narrow streams and gullies to
256 the south, where it is close to the Paka Porphyritic Granite, and the east, where it is
257 adjacent to the King Granite.

258 *Dykes*

259 Pyroxene monzonite dykes form large ENE-WSW trending intrusions up to 20 m wide.
260 On the west face of the mountain individual dykes can be traced for approximately 1 km
261 vertically. Preferential erosion of the dykes is the cause of a number of large, linear
262 depressions across the plateau and many of the gaps between the Diwali Pinnacles of
263 the Western Plateau (Fig. 10h). These dykes contain porphyritic clinopyroxene and K-
264 feldspar in a groundmass of quartz and feldspar. Some dykes were found with subhedral

265 to euhedral tabular K-feldspar phenocrysts ≤ 15 mm long oriented parallel to their
266 margins.

267 **Discussion**

268 The new field evidence allows us to reinterpret the emplacement history and
269 mechanisms of the Mount Kinabalu pluton and its internal structure. The data allows
270 investigation of the pluton and individual unit volumes; the syn-magmatic tectonic
271 setting; the magmatic emplacement mechanisms; and the individual units' spatial and
272 temporal relationships. Based on this we consider the implications for magma
273 emplacement processes.

274 *Pluton thickness*

275 Although the new geological map and contact geometry data allow interpretation of the
276 three dimensional structure of the pluton (Fig. 6 and 7), the basal geometry is not
277 exposed and an independent methodology must be used to assess our interpretations.
278 Cruden & McCaffrey (2001) have proposed that a power law relates the thickness and
279 length of laccoliths, plutons and batholiths:

$$280 \quad T = 0.6(\pm 0.15)L^{0.6(\pm 0.1)} \quad [\text{Equation 1}]$$

281 Importantly, Cruden & McCaffrey (2001) postulated that Equation 1 is consistent for all
282 scales of pluton emplacement including individual bodies and large composite plutons.
283 If this relationship is applicable to Mount Kinabalu then the 11.5 km equivalent circle
284 diameter of the short (9 km) and long (15 km) axes predicts a pluton thickness of 2.6 km
285 (± 1.5 km). This thickness estimate implies that the intrusion does not continue far
286 beneath the observed 2.9 km vertical range of outcrops. Estimates of the volume of
287 granitic material eroded by glaciation based on the glacial till around the pluton
288 concluded that the original uppermost surface of the pluton was unlikely to be much
289 higher than the present summit pinnacles (Sperber 2009). Combining these
290 interpretations suggests that most of the intrusion's original thickness is both exposed
291 and preserved, in agreement with Reinhard & Wenk (1951).

292 *Individual unit volumes*

293 Based on the field data described above, pre-erosional volumetric estimates can be
294 made for each of Mt Kinabalu's composite units (summarised in Table 1 and Fig. 7).

295 Both the upper and lower contacts of the Alexandra Tonalite/Granodiorite were
296 observed in the field, so a good estimate of the unit's thickness can be made (~0.2 km).
297 However it is unclear how much of its lateral extent has been lost to erosion. Equation 1
298 describes the relationship between an intrusion's width and thickness, predicting a
299 lateral unit extent of 0.1 km (0.06-0.3 km within error). The unit has an equivalent circle
300 diameter of 1.3 km, greater than the predicted lateral width, so it is unlikely much
301 material is missing laterally. The unit has an ellipsoidal form in the field (Fig. 7), so
302 modelling it as an ellipsoid with the observed dimensions equates to a total volume of
303 0.2 km³.

304 The upper and lower contacts of the Low's Granite on the Western Plateau were also
305 observed, so the same methodology can be applied as for the previous unit.
306 Extrapolating the contact surfaces (Fig. 6) predicts a unit thickness of ~0.6 km,
307 corresponding to an intrusion width of 1.1 km (0.7-1.6 km within error) according to
308 Equation 1. The unit's outcrop extent has an equivalent circle diameter of 2.3 km,
309 indicating that little material has been lost laterally. Again modelling the unit as an
310 ellipsoid (Fig. 7) gives a unit volume of ~2 km³.

311 The extent and structure of the Low's Granite on the northern flank of the pluton (Fig. 3)
312 are highly ambiguous and poorly constrained, although outcrops were observed over a
313 500 m vertical range. Modelling the unit as an ellipsoid and calculating its thickness using
314 Equation 1 predicts a volume of ~3.9 ±0.5 km³, although this is highly speculative
315 compared to the other units.

316 The King Granite has a more irregular structure than the preceding units of the Western
317 Plateau, and its basal contact is not observed. However, its eastern contact on the
318 Eastern Plateau dips west beneath the intrusion, allowing interpretation of its basal
319 surface (Fig. 6). This estimates a thickness of ~2.3 km, comparable to the 2.2 km
320 predicted by Equation 1. Modelling the unit as an ellipsoid gives a unit volume of ~90
321 km³.

322 The Donkey Granite is well constrained in its length and width, and although it was
323 observed 600m below the plateaux in Low's Gully, it is unclear how far it continues at
324 depth. Allowing a further 200 m and modelling the unit as a cuboid sheet (Fig. 7) equates
325 to a volume of 0.4 km³.

326 The structure of the Paka Porphyritic Granite is irregular as it intruded around the King
327 Granite (Fig. 7), and the form of its basal contact cannot be predicted. However, although
328 the outcrop width varies from 0.2-1.5 km around the pluton, it is most commonly around
329 800 m and so we model it here as a sheet (Fig. 6). This is supported by the dip of the
330 outer western contact beneath the pluton (Fig. 3), implying the unit doesn't widen at
331 depth, and the previous calculation that based on Equation 1 most of the pluton's
332 thickness is exposed. Based on these interpretations we predict a unit volume of ~40
333 km³.

334 The basal structure of the Mesilau Porphyritic Granite is again ambiguous and
335 unexposed. Based on the lateral extent of the unit, Equation 1 predicts a thickness of 1.9
336 km, comparable to the 1.9 km thickness predicted by interpreting a regular basal surface
337 along the pre-emplacement interface of the basement and cover rock (Fig. 6). This is
338 again supported by the previous interpretation based on Equation 1 that the pluton does
339 not continue far at depth. Based on this interpretation of a regular basal surface, the
340 structure of the unit in the field appears to resemble a spherical cap thickening laterally
341 towards its centre (Fig. 6 and 7). Modelling the unit as such predicts a volume of ~40 km³.

342 *Emplacement conditions*

343 Vogt & Flower (1989) employed an Al-in-hornblende geobarometer to estimate
344 emplacement pressures of 1-3 kbar (equivalent to 3-10 km) for the Alexandra
345 Tonalite/Granodiorite and the Low's and King Granites. This estimation has been
346 improved by combining ⁴⁰Ar/³⁹Ar, zircon fission track and (U-Th-Sm)/He
347 thermochronometry to give an upper to mid-crustal emplacement depth of 7-12km
348 (Cottam *et al.* 2013).

349 Metamorphic temperatures in country rocks can be used to estimate the minimum
350 emplacement temperature of an intrusion. Talc and anthophyllite formed by contact

351 metamorphism of ultramafic bodies imply temperatures of 630-700°C at emplacement
352 pressures of 2-3 kbar (Bucher & Grapes 2011). Talc is absent from ultramafic samples far
353 from the contact, indicating that these are contact metamorphic phases. The
354 temperature range overlaps the 470-650°C implied by a hornfels containing coexisting
355 muscovite, biotite and cordierite near the intrusive contact (Bucher & Grapes 2011).
356 These temperatures are consistent with low pressure melting experiments (2-3 kbar)
357 indicating a whole rock solidus of ~670-700°C for granitoids of a similar mineralogical and
358 chemical composition to the main granitic units of Mt Kinabalu (Naney 1983, Lambert &
359 Wyllie 1974, Klimm *et al.* 2003, Holtz & Johannes 1994). The presence of hornblende at
360 these temperatures implies high H₂O contents (>5 wt.%; Bogaerts *et al.* 2006).

361 *Accommodation space*

362 Whether melt emplacement was accommodated through roof lifting or floor depression
363 differentiates laccolithic and lopolithic emplacement mechanisms and can be
364 determined from country rock structures. Sedimentary beds >1.9 km to the north, south,
365 southwest and southeast of Mt Kinabalu dip towards the south and/or west (dominantly
366 southwest), reflecting deformation of the Crocker sediments prior to the intrusion of Mt
367 Kinabalu. However, beds closer to the pluton strike sub parallel to the contact and dip
368 away from the pluton. This reorientation of the country rock structures implies that the
369 sedimentary units bow upwards over the pluton (Fig. 6) with accommodation space
370 created through upward deformation and roof lifting of the overlying sediments in a
371 laccolith style, although floor depression may also have occurred (Cruden 1998). Earlier
372 units were also tilted by each subsequent intrusion, producing the westward inclination
373 of the Alexandra Tonalite/Granodiorite and Low's Granite contact surfaces. The intrusion
374 was emplaced at the contact of the basement sedimentary cover rocks, and it was likely
375 this interface that halted magma ascent and determined the depth of emplacement
376 (Clemens & Mawer 1992).

377 *Internal structure and implications for pluton emplacement mechanisms*

378 In current models of composite pluton growth, successive pulses intrude above or below
379 their predecessors as horizontal tabular bodies (Cruden 1998, Cruden 2006, Grocott *et al.*
380 2009). The exhumation and preservation of peripheral material at Mt Kinabalu

381 provides a unique opportunity to observe the three dimensional internal structure of a
382 pluton and to test this model of composite pluton growth.

383 The initial two units have tabular forms suggesting that magma spread laterally upon
384 reaching its emplacement level (Fig. 7); the second (Low's Granite) emplaced below the
385 first (Alexandra Tonalite/Granodiorite). This closely resembles the sheeted laccolith
386 model (Cruden 1998, Cruden 2006, Wiebe & Collins 1998, de Saint-Blanquat *et al.* 2006)
387 as previously advocated for Mt Kinabalu (Cottam *et al.* 2010). However, these early units
388 diverge slightly from the general model as the Low's Granite ascended around the sides
389 of the Alexandra Tonalite/Granodiorite and enveloped its periphery (Fig. 7). Further
390 upward deformation accommodated the King Granite, tilting both the earlier intrusions
391 and their overburden (Fig. 6) in a similar manner to other composite plutons (Stevenson
392 *et al.* 2007, Grocott *et al.* 2009). The King Granite formed a major impediment for the
393 upwelling Paka Porphyritic Granite magma which (unlike the Donkey Granite) was unable
394 able to ascend through the now-crystallised body. Unable to deform or uplift the earlier
395 bodies but still experiencing positive buoyancy, the Paka Porphyritic Granite ascended
396 around the periphery of the earlier units (Fig. 6 and 7) rather than extending laterally at
397 the same crustal level they had exploited. Finally, again restricted by the earlier units,
398 the Mesilau Porphyry intruded beneath the intrusion and extended laterally to the SE
399 (Fig. 7).

400 Mt Kinabalu highlights the effect of pre-existing granite pseudo-stratigraphy on magma
401 emplacement, producing a complex internal structure (Fig. 7). Instead of the intrusion of
402 each pulse being independent of those before, emplacement was affected by the
403 structure and crystallisation state of the earlier intrusions. At any instant the existing
404 structure controlled the spatial distribution of subsequent intrusions, forcing later pulses
405 in a particular direction with the granite-country rock contacts of earlier units being
406 intruded preferentially over the original emplacement depth of the sediment-ophiolite
407 contact.

408 *Tectonic setting*

409 Dyke and fault orientations were recorded from within the pluton to determine the syn-
410 magmatic tectonic setting and associated paleostresses (Fig. 11), although shear sense

411 indicators were largely lacking. In both compressive and extensional regimes, dykes will
412 propagate perpendicular to the direction of minimum compressive stress (σ_3), parallel
413 to the plane containing the maximum (σ_1) and intermediate (σ_2) compressive stresses
414 (Fig. 12a and 12 c). In contrast, all shear fractures (faults) will propagate obliquely to σ_1
415 and in an extensional regime will strike parallel to σ_2 (Fig. 12b and 12d; Bles & Feuga
416 1986, Park 1997). Consequently, in extensional regimes (i.e. where σ_1 is vertical) faults
417 and dykes will share similar strike orientations, whilst in compressive regimes (i.e. where
418 σ_1 is not vertical) the two populations will have different strike orientations (Fig. 12).

419 Measurements from faults and both aplite and intrusive dykes (dominantly pyroxene
420 monzonite) show dominantly steep dips and similar strike orientations trending ENE-
421 WSW (Fig. 11), as would be expected in an extensional regime (Fig. 12a and 12b). A
422 limited number of shear sense indicators were observed but showed no preferred
423 orientation or sense of movement.

424 Although the faults and pyroxene monzonite dykes have not been dated and may
425 significantly post-date intrusion of the Mt Kinabalu pluton, aplite dykes are
426 contemporaneous with the pluton as they are generated from residual, highly
427 fractionated interstitial melts infilling extensional fractures during the crystallisation and
428 contraction of their granitic host (Best 2003). Consequently the steeply NNW-SSE dipping
429 orientation of the aplite dykes indicates a subhorizontal NNW-SSE oriented σ_3 direction
430 (Fig. 11). The ENE-WSW strike of the aplite dykes is shared by both the faults and
431 pyroxene monzonite dykes, so the subhorizontal NNW-SSE orientation of σ_3 can be
432 interpreted to continue during and after intrusion of the pluton. It should be noted,
433 however, that whilst the fault and pyroxene monzonite dyke orientations are largely
434 concentrated in a common ENE-WSW strike (Fig. 11), the aplite dyke orientations are
435 more dispersed. As aplites are formed during the crystallisation and contraction of their
436 host pluton this is likely the result of localised stresses produced by the contraction being
437 superimposed on the regional stress field. These localised stresses may also explain the
438 more minor dispersed orientations of the faults and pyroxene monzonite dykes.

439 In contrast with the interpretation of the regional stress field from the field data, the
440 intrusion of magma in to the crust can perturb the local stress field during emplacement

441 (Vigneresse *et al.* 1999). However, the stresses induced by magma emplacement
442 produce fractures and dykes whose strikes radiate from or are concentric around the
443 central point of emplacement induced pressure (likely the core of the pluton or dyke,
444 Castro 1984). The dyke and fault orientations of Mt Kinabalu do not show such a
445 distribution, indicating their formation was influenced by regional stresses not perturbed
446 by local syn-emplacement stresses. Furthermore, any stresses related to magmatic
447 emplacement superimposed on the regional stress field would wane following
448 emplacement, resulting in different interpreted stress directions for the aplite dykes
449 (shortly after emplacement) and faults (later post emplacement) which is not the case
450 (Fig. 11).

451 These observations indicate NNW-SSE orientated regional extension during
452 emplacement of the pluton (the σ_3 direction), supporting previous interpretations
453 (Cottam *et al.* 2013, Hall 2013) that the emplacement and uplift of the pluton was
454 associated with contemporaneous crustal extension. Vogt & Flower (1989) and Swauger
455 *et al.* (2000) ascribed melt generation and uplift to compression and crustal thickening
456 associated with the Sabah Orogeny. However, the revised Late Miocene ages for the
457 emplacement and uplift of the pluton (Cottam *et al.* 2013, Cottam *et al.* 2010)
458 significantly post-date this Early Miocene collisional event (Hutchison 1996, Balaguru &
459 Nichols 2004, Hall *et al.* 2008). Post-orogenic extension affected sediments elsewhere in
460 northern Borneo (Hutchison 2000) and may be associated with Miocene extension of the
461 Sulu Sea basin (Hall 2013), NE of Sabah (Fig. 1). The structural data presented here
462 provides evidence for extension in northern Sabah during the Late Miocene, extending
463 the duration and extent of Miocene extension in Borneo. Further evidence should be
464 sought to determine the extent of Late Miocene extension and to prove that this is not
465 purely local extension, as this conclusion implies that tectonic models interpreting the
466 region as in a compressive regime following the cessation of South China Sea spreading
467 (e.g. King *et al.* 2010, Pubellier & Morley 2013) require revaluation.

468 **Conclusions**

469 The Mt Kinabalu granitic intrusion was emplaced in the upper to middle crust over ~0.8
470 My in the Late Miocene. The pluton was emplaced in a regional extensional setting, and

471 steeply NNW-SSE dipping dyke and fault orientations suggest a NNW-SSE oriented
472 regional extension direction challenging tectonic models that predict contemporaneous
473 regional compression. The composite Mt Kinabalu intrusion comprises six major units:
474 the oldest unit being a tonalite/granodiorite, followed by three subsequent sub-
475 equigranular granites and two final porphyritic granites (not quartz monzonite as
476 previously suggested). The changing compositions of these composite units reflect an
477 evolving system of magmatic fractionation and assimilation (Burton-Johnson 2013)
478 which will be discussed in a future paper.

479 Magma was emplaced along the contact of the ultramafic basement and sedimentary
480 overburden where the contact interface halted upward magma migration and initiated
481 lateral intrusion. Emplacement was accommodated by roof uplift and flexure of the
482 overlying sediments, although floor depression may also have occurred. Successive
483 magmatic units were largely emplaced beneath each other. Each successive pulse tilted
484 earlier units, intruded around them and enveloped their periphery, exploiting the
485 granite-country rock contacts of previous units in preference to the basement-cover rock
486 contact exploited by earlier units. This produced an irregular three dimensional internal
487 structure, deviating somewhat from tabular intrusive emplacement models and
488 providing insight in to the 3D structure of composite intrusive bodies.

489 **Acknowledgements**

490 This study was funded by the Natural Environment Research Council as part of a PhD
491 Research Project. We would like to thank Sandy Cruden and Michel de Saint-Blanquat for
492 their helpful and thorough reviews of our submitted manuscript. In addition we wish to
493 thank Alim Biun, Felix Tongkul and Maklarin Lakim for their assistance in facilitating the
494 field season; Jamili Nais of Sabah Parks who allowed us to work in the National Park; Kate
495 Saunders for her help with the DEM; the mountain guides and researchers of Mt Kinabalu
496 National Park, especially Alijen “Jen”, Halli, Jasirin, Sokaibin, Maklarin Lakim, Sapinus,
497 Samuel and Nicholas; and we thank the SE Asia Research Group at Royal Holloway for
498 their support throughout this project. We also kindly acknowledge Mike Cottam, Christian
499 Sperber and Antony van der Ent for their assistance, discussions and field material.

- 500 BALAGURU, A. & NICHOLS, G. 2004. Tertiary stratigraphy and basin evolution, southern
501 Sabah (Malaysian Borneo). *Journal of Asian Earth Sciences*, **23**, 537–554, doi:
502 10.1016/j.jseaes.2003.08.001.
- 503 BALAGURU, A., NICHOLS, G. & HALL, R. 2003. Tertiary stratigraphy and basin evolution of
504 southern Sabah: implications for the tectono-stratigraphic evolution of Sabah,
505 Malaysia. *Bulletin of the Geological Society of Malaysia*, **47**, 27–49.
- 506 BEST, M.G. 2003. *Igneous and Metamorphic Petrology*. Malden, MA, USA, Blackwell
507 Publishing.
- 508 BLES, J.L. & FEUGA, B. 1986. *The Fracture of Rocks*. New York, USA, Elsevier Science B.V.
- 509 BOGAERTS, M., SCAILLET, B. & AUWERA, J.V. 2006. Phase Equilibria of the Lyngdal
510 Granodiorite (Norway): Implications for the Origin of Metaluminous Ferroan
511 Granitoids. *Journal of Petrology*, **47**, 2405–2431, doi: 10.1093/petrology/egl049.
- 512 BUCHER, K. & GRAPES, R. 2011. *Petrogenesis of Metamorphic Rocks*, 8th Edition.
513 Heidelberg, Germany, Springer.
- 514 BURTON-JOHNSON, A. 2013. *Origin, Emplacement and Tectonic Relevance of the Mt.*
515 *Kinabalu Granitic Pluton of Sabah, Borneo*. Durham University.
516 <http://etheses.dur.ac.uk/9450/>.
- 517 CASTRO, A. 1984. Emplacement fractures in granite plutons (Central Extremadura
518 batholith, Spain). *Geologische Rundschau*, **73**, 869–880.
- 519 CLEMENS, J.D. & MAWER, C.K. 1992. Granitic magma transport by fracture propagation.
520 *Tectonophysics*, **204**, 339–360, doi: 10.1016/0040-1951(92)90316-X.
- 521 COLLENETTE, P. 1958. *The Geology and Mineral Resources of the Jessleton-Kinabalu Area,*
522 *North Borneo*. Kuching, Srawak, Geological Survey Department, British Territories
523 in Borneo.
- 524 COLLENETTE, P. 1965. The geology and mineral resources of the Pensiangan and Upper
525 Kinabatangan area, Sabah. *Malaysia Geological Survey Borneo Region, Memoir*
526 *12*, 150.
- 527 COTTAM, M.A., HALL, R., SPERBER, C. & ARMSTRONG, R. 2010. Pulsed emplacement of the
528 Mount Kinabalu granite, northern Borneo. *Journal of the Geological Society*, **167**,
529 49–60, doi: 10.1144/0016-76492009-028.Pulsed.
- 530 COTTAM, M.A., HALL, R., SPERBER, C., KOHN, B.P., FORSTER, M.A. & BATT, G.E. 2013. Neogene
531 rock uplift and erosion in northern Borneo: evidence from the Kinabalu granite,
532 Mount Kinabalu. *Journal of the Geological Society*, **170**, 805–816, doi:
533 10.1144/jgs2011-130.
- 534 CRUDEN, A.R. 1998. On the emplacement of tabular granites. *Journal of the Geological*
535 *Society*, **155**, 853–862.

- 536 CRUDEN, A.R. 2006. Emplacement and growth of plutons: implications for rates of melting
537 and mass transfer in continental crust. *In: Evolution and Differentiation of the*
538 *Continental Crust*. Cambridge, UK, Cambridge University Press.
- 539 CRUDEN, A.R. & McCAFFREY, K.J.W. 2001. Growth of plutons by floor subsidence:
540 implications for rates of emplacement, intrusion spacing and melt-extraction
541 mechanisms. *Physics and Chemistry of the Earth, Part A: Solid Earth and Geodesy*,
542 **26**, 303–315, doi: 10.1016/S1464-1895(01)00060-6.
- 543 CULLEN, A.B. 2010. Transverse segmentation of the Baram-Balabac Basin, NW Borneo:
544 refining the model of Borneo's tectonic evolution. *Petroleum Geoscience*, **16**, 3–
545 29, doi: 10.1144/1354-079309-828.
- 546 DE SAINT-BLANQUAT, M., LAW, R.D., BOUCHEZ, J.-L. & MORGAN, S.S. 2001. Internal structure
547 and emplacement of the Papoose Flat pluton: An integrated structural,
548 petrographic, and magnetic susceptibility study. *Geological Society of America*
549 *Bulletin*, **113**, 976–995.
- 550 DE SAINT-BLANQUAT, M., HABERT, G., HORSMAN, E., MORGAN, S.S., TIKOFF, B., LAUNEAU, P. &
551 GLEIZES, G. 2006. Mechanisms and duration of non-tectonically assisted magma
552 emplacement in the upper crust: the Black Mesa pluton, Henry Mountains, Utah.
553 *Tectonophysics*, **428**, 1–31.
- 554 DE SILVA, S.L. & GOSNOLD, W.D. 2007. Episodic construction of batholiths: insights from the
555 spatiotemporal development of an ignimbrite flare-up. *Journal of Volcanology*
556 *and Geothermal Research*, **167**, 320–335.
- 557 DHONAU, T.J. & HUTCHISON, C.S. 1965. The Darvel Bay area, East Sabah, Malaysia. *Malaysia*
558 *Geological Survey Borneo Region, Annual Report for 1965*, 141–160.
- 559 GROCOTT, J., ARÉVALO, C., WELKNER, D. & CRUDEN, A.R. 2009. Fault-assisted vertical pluton
560 growth: Coastal Cordillera, north Chilean Andes. *Journal of the Geological Society*,
561 **166**, 295–301.
- 562 HALL, R. 1996. Reconstructing Cenozoic SE Asia. *In: Hall, R. & Blundell, D. J. (eds) Tectonic*
563 *Evolution of SE Asia*. Geological Society, London, Special Publications, **106**, 153–
564 184.
- 565 HALL, R. 2013. Contraction and extension in northern Borneo driven by subduction
566 rollback. *Journal of Asian Earth Sciences*, **76**, 399–411, doi:
567 10.1016/j.jseae.2013.04.010.
- 568 HALL, R. & WILSON, M.E.J. 2000. Neogene sutures in eastern Indonesia. *Journal of Asian*
569 *Earth Sciences*, **18**, 781–808.
- 570 HALL, R., VAN HATTUM, M.W. A. & SPAKMAN, W. 2008. Impact of India–Asia collision on SE
571 Asia: The record in Borneo. *Tectonophysics*, **451**, 366–389, doi:
572 10.1016/j.tecto.2007.11.058.

- 573 HAZEBROEK, H.P. & TAN, D.N.K. 1993. Tertiary tectonic evolution of the NW Sabah
574 continental margin. *Bulletin of the Geological Society of Malaysia*, **33**, 195–210.
- 575 HOLTZ, F. & JOHANNES, W. 1994. Maximum and minimum water contents of granitic melts:
576 implications for chemical and physical properties of ascending magmas. *Lithos*,
577 **32**, 149–159.
- 578 HORSMAN, E., MORGAN, S., DE SAINT-BLANQUAT, M., HABERT, G., NUGENT, A., HUNTER, R.A. &
579 TIKOFF, B. 2009. Emplacement and assembly of shallow intrusions from multiple
580 magma pulses, Henry Mountains, Utah. *Earth and Environmental Science*
581 *Transactions of the Royal Society of Edinburgh*, **100**, 117–132.
- 582 HUTCHISON, C. 1978. Ophiolite metamorphism in northeast Borneo. *Lithos*, 195–208.
- 583 HUTCHISON, C. 2000. A Miocene collisional belt in north Borneo: uplift mechanism and
584 isostatic adjustment quantified by thermochronology. *Journal of the Geological*
585 *Society*, **157**, 783–793.
- 586 HUTCHISON, C.S. 1996. The ‘Rajang accretionary prism’ and ‘Lupar Line’ problem of
587 Borneo. *Geological Society, London, Special Publications*, **106**, 247–261, doi:
588 10.1144/GSL.SP.1996.106.01.16.
- 589 HUTCHISON, C.S. 2005. *Geology of North-West Borneo: Sarawak, Brunei and Sabah*.
590 Elsevier.
- 591 IMAI, A. & OZAWA, K. 1991. Tectonic implications of the hydrated garnet peridotites near
592 Mt Kinabalu, Sabah, East Malaysia. *Journal of Southeast Asian Earth Sciences*, **6**,
593 431–445.
- 594 JACOBSON, G. 1970. *Gunung Kinabalu Area, Sabah, Malaysia*. Kuching, Sarawak, Geological
595 Survey Malaysia.
- 596 KASAMA, T., AKIMOTO, H., HADA, S. & JACOBSON, G. 1970. Geology of the Mt. Kinabalu area,
597 Sabah, Malaysia. *Journal of Geosciences, Osaka City University*, **13**, 113–148.
- 598 KING, R.C., BACKÉ, G., MORLEY, C.K., HILLIS, R.R. & TINGAY, M.R.P. 2010. Balancing
599 deformation in NW Borneo: Quantifying plate-scale vs. gravitational tectonics in
600 a delta and deepwater fold-thrust belt system. *Marine and Petroleum Geology*,
601 **27**, 238–246, doi: 10.1016/j.marpetgeo.2009.07.008.
- 602 KIRK, H.J.C. 1968. *The Igneous Rocks of Sarawak and Sabah*. US Government Printing
603 Office.
- 604 KLIMM, K., HOLTZ, F., JOHANNES, W. & KING, P.L. 2003. Fractionation of metaluminous A-type
605 granites: an experimental study of the Wangrah Suite, Lachlan Fold Belt,
606 Australia. *Precambrian Research*, **124**, 327–341.

- 607 KOOPMANS, B.N. 1967. Deformation of the metamorphic rocks and the Chert–Spilite
608 Formation in the southern part of the Darvel Bay area, Sabah. *Geological Survey*
609 *of Malaysia, Borneo Region, Bulletin*, **8**, 14–24.
- 610 LAMBERT, I.B. & WYLLIE, P.J. 1974. Melting of tonalite and crystallization of andesite liquid
611 with excess water to 30 kilobars. *The Journal of Geology*, 88–97.
- 612 LEONG, K.M. 1974. *The Geology and Mineral Resources of the Upper Segama Valley and*
613 *Darvel Bay Area, Sabah, Malaysia*. US Government Printing Office.
- 614 McCAFFREY, K.J.W. & PETFORD, N. 1997. Are granitic intrusions scale invariant? *Journal of*
615 *the Geological Society*, **154**, 1–4, doi: 10.1144/gsjgs.154.1.0001.
- 616 MORLEY, C.K. & BACK, S. 2008. Estimating hinterland exhumation from late orogenic basin
617 volume, NW Borneo. *Journal of the Geological Society*, **165**, 353–366.
- 618 NANEY, M. 1983. Phase equilibria of rock-forming ferromagnesian silicates in granitic
619 systems. *American Journal of Science*.
- 620 NEWTON-SMITH, J. 1967. *Bidu-Bidu Hills Area: Sabah, East Malaysia*. Geological Survey,
621 Geological Survey of Malaysia, Borneo Region, Bulletin 4.
- 622 NOAD, J.J. 1998. *The Sedimentary Evolution of the Tertiary of Eastern Sabah, Northern*
623 *Borneo*. PhD Thesis, Birkbeck, University of London.
- 624 OMANG, S. A. K. & BARBER, A. J. 1996. Origin and tectonic significance of the metamorphic
625 rocks associated with the Darvel Bay Ophiolite, Sabah, Malaysia. *Geological*
626 *Society, London, Special Publications*, **106**, 263–279, doi:
627 10.1144/GSL.SP.1996.106.01.17.
- 628 PARK, R.G. 1997. *Foundations of Structural Geology*. London, UK, Routledge.
- 629 PETFORD, N. & CLEMENS, J. 2000. Granites are not diapiric! *Geology Today*, 180–184.
- 630 PETFORD, N., CRUDEN, A.R., McCAFFREY, K.J. & VIGNERESSE, J.L. 2000. Granite magma
631 formation, transport and emplacement in the Earth’s crust. *Nature*, **408**, 669–
632 673, doi: 10.1038/35047000.
- 633 PUBELLIER, M. & MORLEY, C.K. 2013. The Basins of Sundaland (SE Asia); evolution and
634 boundary conditions. *Marine and Petroleum Geology*.
- 635 RANGIN, C. & SILVER, E.A. 1990. Geological setting of the Celebes and Sulu Seas. *In*: Silver,
636 E. A., Rangin, C. & von Breyman, M. T. (eds) *Proceedings of the Ocean Drilling*
637 *Program, Initial Reports* 124. 35–42.
- 638 REINHARD, M. & WENK, E. 1951. Geology of the Colony of North Borneo. *British Borneo*
639 *Geological Survey Bulletin*, **1**.
- 640 SANDAL, S.T. (ed.). 1996. *The Geology and Hydrocarbon Resources of Negara Brunei*
641 *Darussalam*. Brunei Museum, Syabas Bandar Seri Begawan, Brunei Darussalam.

- 642 SPERBER, C. 2009. *The Thermotectonic Development of Mount Kinabalu, Sabah, Malaysia:*
643 *Constraints from Low-Temperature Thermochronology*. PhD Thesis, Royal
644 Holloway, University of London.
- 645 STEVENSON, C.T.E., OWENS, W.H., HUTTON, D.H.W., HOOD, D.N. & MEIGHAN, I.G. 2007.
646 Laccolithic, as opposed to cauldron subsidence, emplacement of the Eastern
647 Mourne pluton, N. Ireland: evidence from anisotropy of magnetic susceptibility.
648 *Journal of the Geological Society*, **164**, 99–110, doi: 10.1144/0016076492006-
649 008.
- 650 SWAUGER, D.A., HUTCHISON, C.S., BERGMAN, S.C. & GRAVES, J.E. 2000. Age and emplacement
651 of the Mount Kinabalu pluton. *Geological Society of Malaysia Bulletin*, **44**, 159–
652 163.
- 653 TAYLOR, B. & HAYES, D.E. 1983. Origin and history of the South China Sea basin. *In*: Hayes,
654 D. E. (ed.) *The Tectonic and Geologic Evolution of Southeast Asian Seas and*
655 *Islands: Part 2*. American Geophysical Union, Geophysical Monographs Series, **27**,
656 23–56.
- 657 TONGKUL, F. 1991. Tectonic evolution of Sabah, Malaysia. *Journal of Southeast Asian Earth*
658 *Sciences*, **6**, 395–405.
- 659 TONGKUL, F. 1994. The geology of Northern Sabah, Malaysia: its relationship to the
660 opening of the South China Sea Basin. *Tectonophysics*, **235**, 131–147.
- 661 TONGKUL, F. & CHANG, F.K. 2003. Structural geology of the Neogene Maliau Basin, Sabah.
662 *Bulletin of the Geological Society of Malaysia*, **47**, 51–61.
- 663 VAN HATTUM, M.W., HALL, R., PICKARD, A.L. & NICHOLS, G.J. 2006. Southeast Asian sediments
664 not from Asia: Provenance and geochronology of north Borneo sandstones.
665 *Geology*, **34**, 589–592.
- 666 VIGNERESSE, J.L. 2006. Granitic batholiths: from pervasive and continuous melting in the
667 lower crust to discontinuous and spaced plutonism in the upper crust.
668 *Transactions of the Royal Society of Edinburgh: Earth Sciences*, **97**, 311–324.
- 669 VIGNERESSE, J.L. & CLEMENS, J.D. 2000. Granitic magma ascent and emplacement: neither
670 diapirism nor neutral buoyancy. *Geological Society, London, Special Publications*,
671 **174**, 1–19, doi: 10.1144/GSL.SP.1999.174.01.01.
- 672 VIGNERESSE, J.-L., TIKOFF, B. & AMÉGLIO, L. 1999. Modification of the regional stress field by
673 magma intrusion and formation of tabular granitic plutons. *Tectonophysics*, **302**,
674 203–224.
- 675 VOGT, E. & FLOWER, M. 1989. Genesis of the Kinabalu (Sabah) granitoid at a subduction-
676 collision junction. *Contributions to Mineralogy and Petrology*, 493–509.

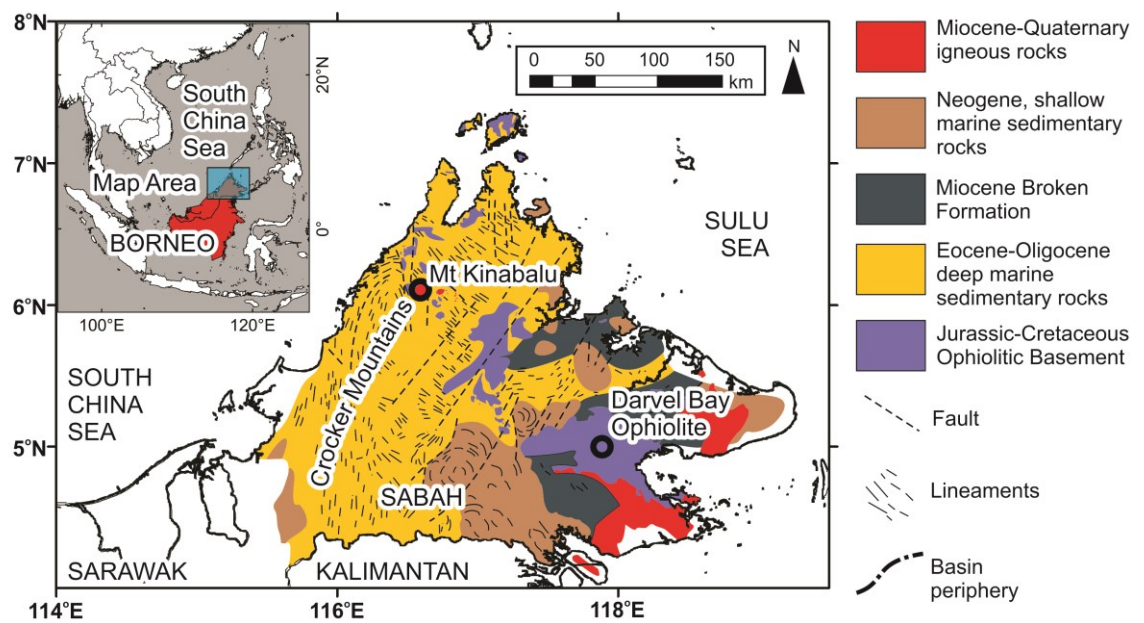
- 677 VOLLMER, F.W. 2015. Orient 3: a new integrated software program for orientation data
678 analysis, kinematic analysis, spherical projections, and Schmidt plots. *In:*
679 *Geological Society of America Abstracts with Programs*. 0.
- 680 WHITNEY, D.L. & EVANS, B.W. 2010. Abbreviations for names of rock-forming minerals.
681 *American mineralogist*, **95**, 185.
- 682 WIEBE, R.A. 1988. Structural and magmatic evolution of a magma chamber: the Newark
683 Island layered intrusion, Nain, Labrador. *Journal of Petrology*, **29**, 383–411.
- 684 WIEBE, R.A. & COLLINS, W.J. 1998. Depositional features and stratigraphic sections in
685 granitic plutons: implications for the emplacement and crystallization of granitic
686 magma. *Journal of Structural Geology*, **20**, 1273–1289.
- 687

Unit	Alexandra Tn/Gd	Low's Gt	King Gt	Donkey Gt	Paka Pph	Mesilau Pph
U-Pb Age (Ma)	7.85 ±0.08	7.69 ±0.07 – 7.64 ±0.11	7.46 ±0.08 – 7.44 ±0.09	7.46 > t > 7.32	7.32 ±0.09 – 7.22 ±0.07	–
Approx. Vol. (Km ³)	0.2	2 (W) 4 (N)	90	0.4	40	40
Phases (Modal %)						
Qz	23-28	16-28	14-27	23	15-21	7-21
Pl	40-45	25-33	21-38	26	23-33	24-28
Kfs	4-7	18-29	26-36	25	23-35	38-48
Hbl	4-13	21-28	9-21	11	11-24	8-23
Bt	9-19	4-7	0-5	13	1-2	0-5
Cpx	–	–	–	–	–	0-2
Accessory	Ap, Ep	Ap, Ep, Zrn	Ap, Ep, Zrn	Ap	Ap	Ap, Spn

688

689 Table 1. Summary of U-Pb zircon ages, estimated volumes and modal mineralogies of the
690 major granitoid units. Abbreviations used: Tn – Tonalite; Gd – Granodiorite; Gt – Granite;
691 Pph – Porphyritic Granite; Qz – Quartz; Pl – Plagioclase; Kfs – Potassium Feldspar; Hbl –
692 Hornblende; Bt – Biotite; Cpx. – Clinopyroxene; Ap – Apatite; Ep – Epidote; Zrn – Zircon;
693 Spn – Sphene (Whitney & Evans 2010).

694



695

696

697 Fig. 1. Simplified geological map of Sabah, adapted from (Kirk 1968), (Balaguru & Nichols
698 2004) and (Hutchison 2005).

699



700

701

702 Fig. 2. Photo of Mt Kinabalu looking north from the town of Kundasang, 10 km south and
703 2800 m below the summit, illustrating the scale, relief and contrast of the forested lower
704 flanks and glaciated summit plateaux of the mountain.

705

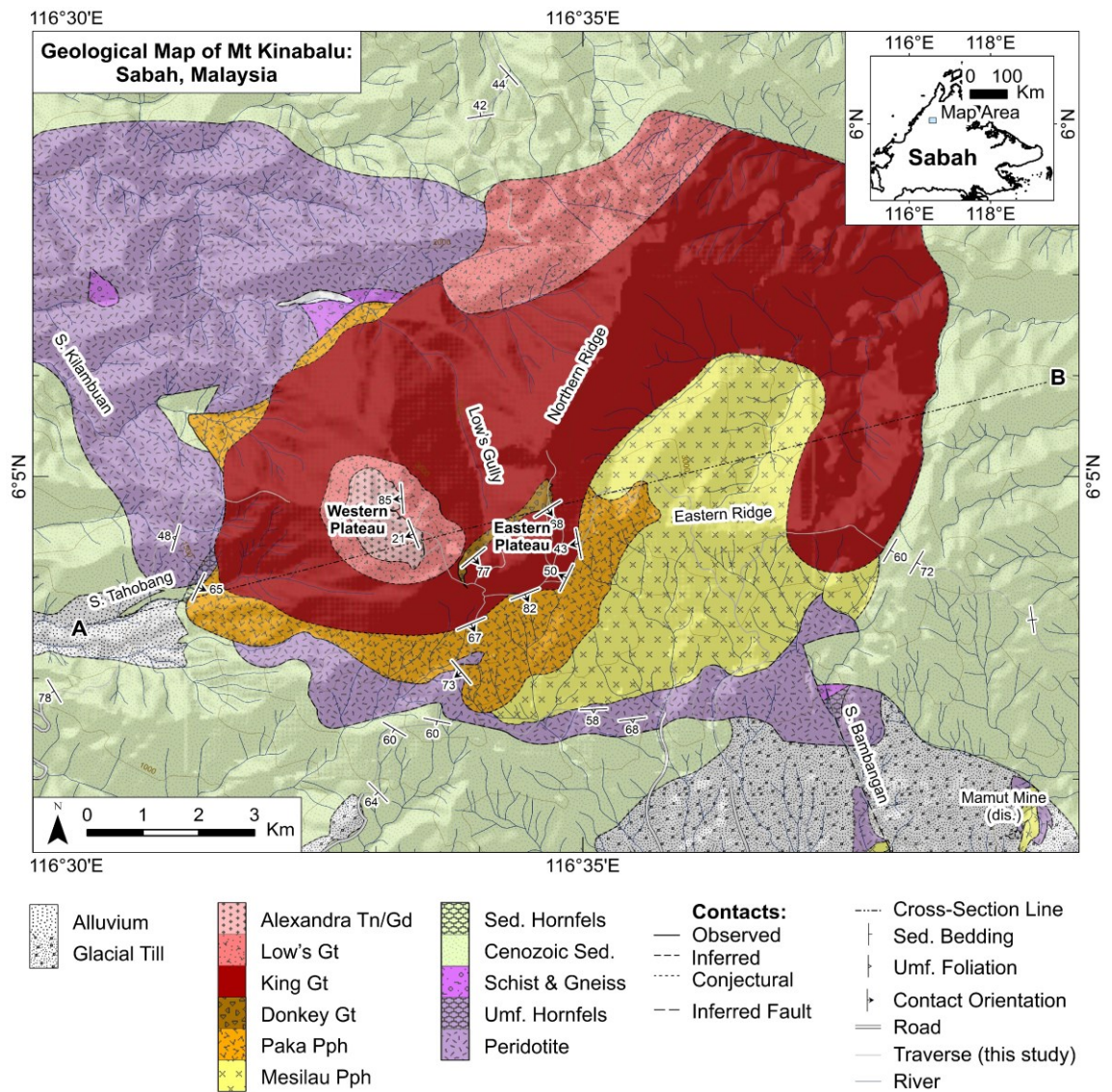
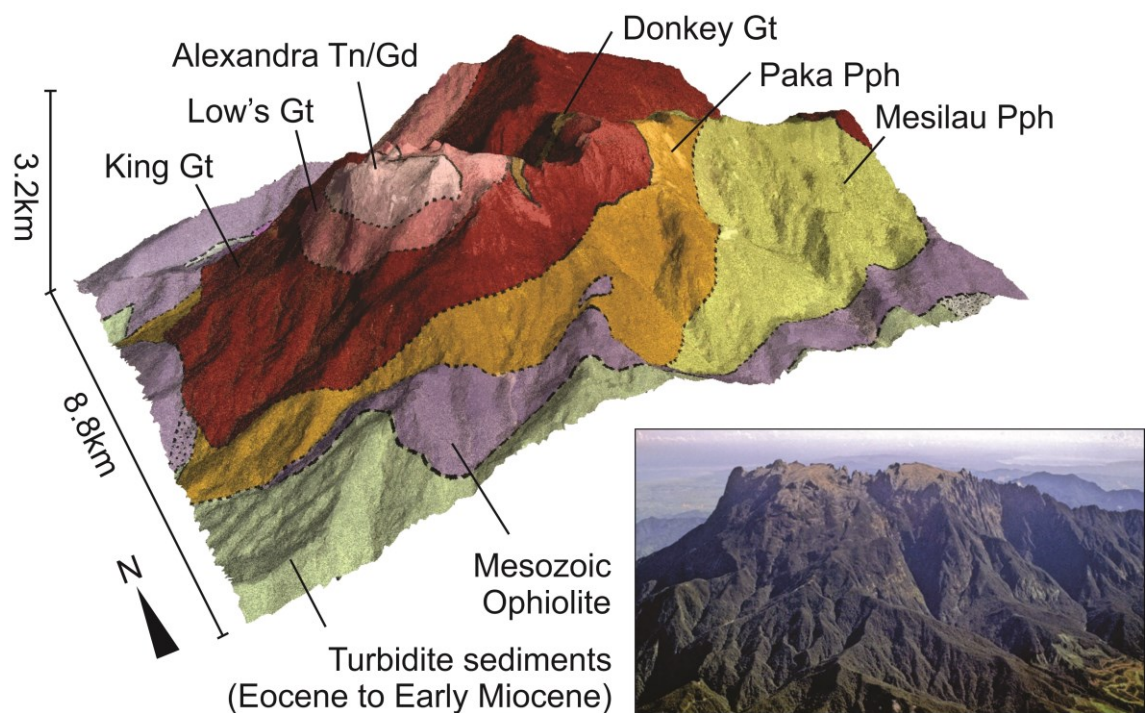


Fig. 3. Geological Map of Mt Kinabalu, combining observations of this study with the map of Jacobson (1970). Inset shows regional geography and study area. Abbreviations used: "S." prefix denotes "Sungai", Malay for "River"; Tn – Tonalite; Gd – Granodiorite; Gt – Granite; Pph – Porphyritic Granite; Sed. – Sedimentary; Umf. – Ultramafic.



713

714

715 Fig. 4. New geological map overlain on the DEM of the mountain and photo from the air
 716 of a similar view for comparison (photo courtesy of Dr Tony Barber, SEARG).
 717 Abbreviations as in Fig. 3. Ages of granitic units from Cottam et al. (2010).

718

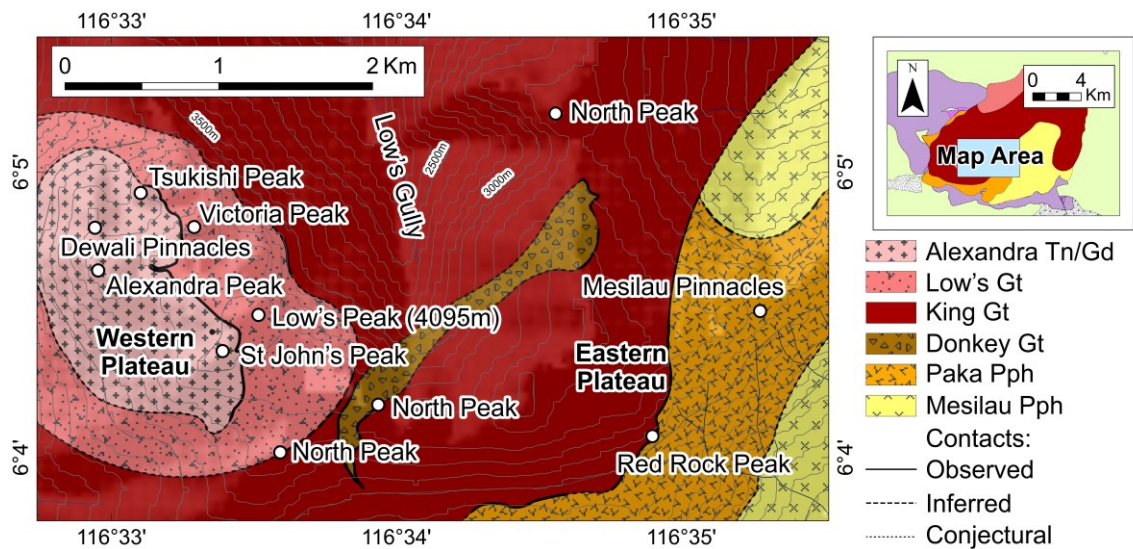
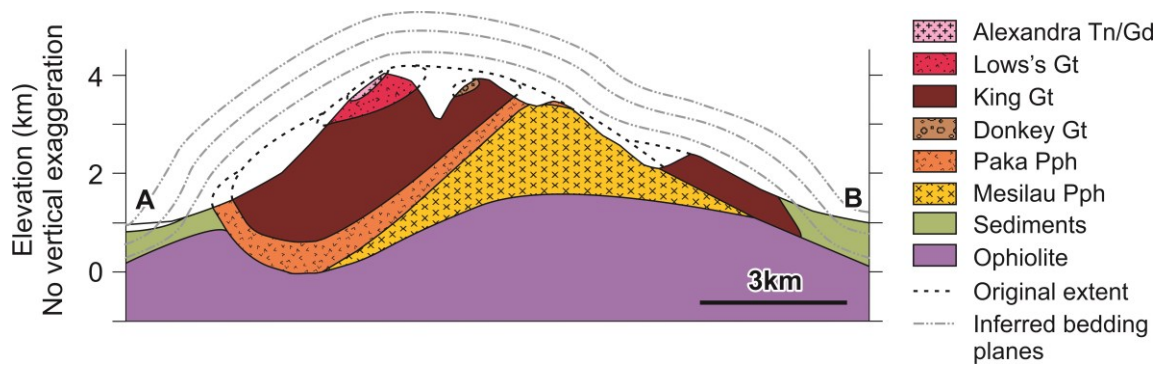


Fig. 5. Summit map of the Western and Eastern plateaux of Mt Kinabalu, separated by Low's Gully, showing the geological interpretation and peak names referred to in the text. Abbreviations as in Fig. 3.

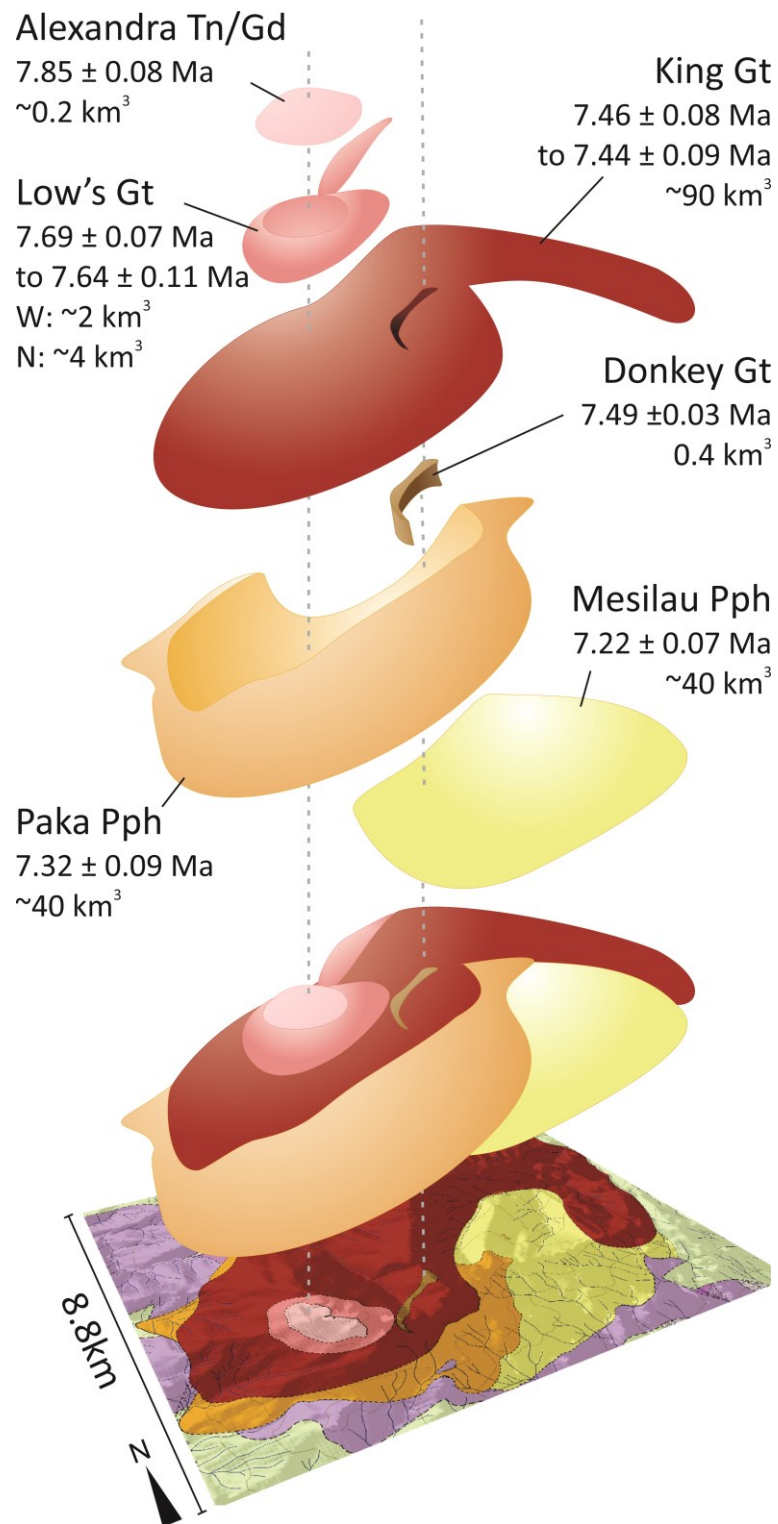


725

726

727 Fig. 6. Interpreted geological cross-sections of the mountain showing the internal
 728 structure of the pluton and extrapolated original extent. Line of section as shown in Fig.
 729 3. No vertical exaggeration.

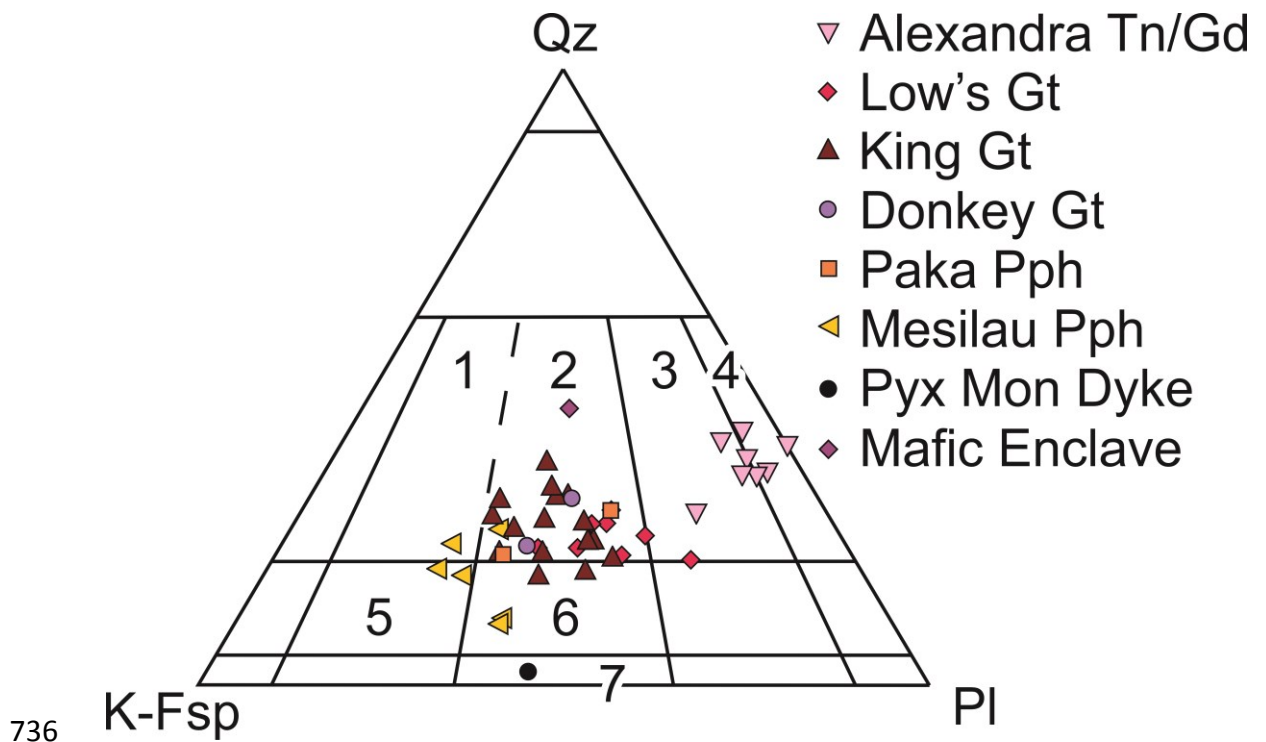
730



731

732 Fig. 7. Exploded view illustration of the pre-erosional structure of the Mt Kinabalu pluton
 733 and its composite units. Emplacement ages from Cottam et al. (2010). Calculated volumes
 734 from Table 1. Abbreviations as in Fig. 3.

735



738 Fig. 8. Classification of the Mt Kinabalu granitoids, according to the modal IUGS-
 739 Streckeisen classification (Streckeisen, 1976). Classification codes: (1) Syenogranite; (2)
 740 Monzogranite; (3) Granodiorite; (4) Tonalite; (5) Quartz-Syenite; (6) Quartz- Monzonite);
 741 (7) Monzonite. Abbreviations as in Fig. 3, plus: Pyx Mon – Pyroxene Monzonite.

742

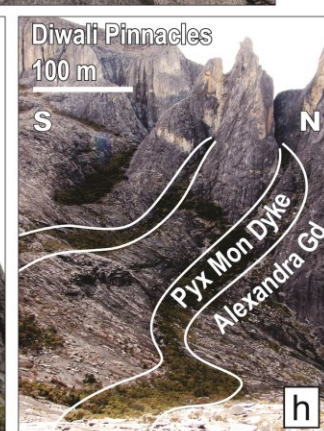
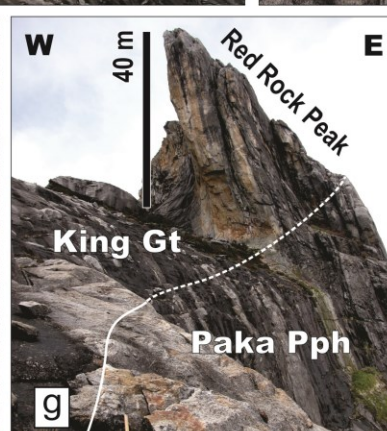
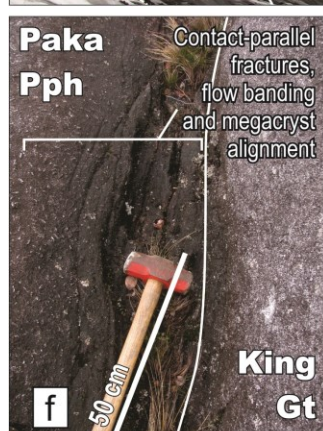
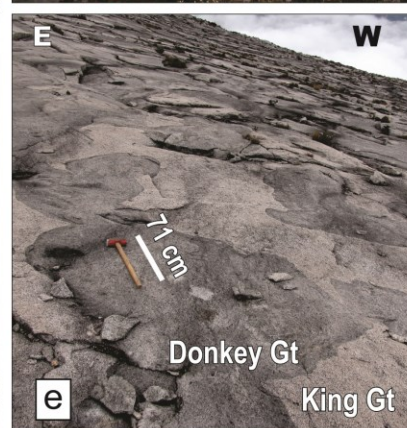
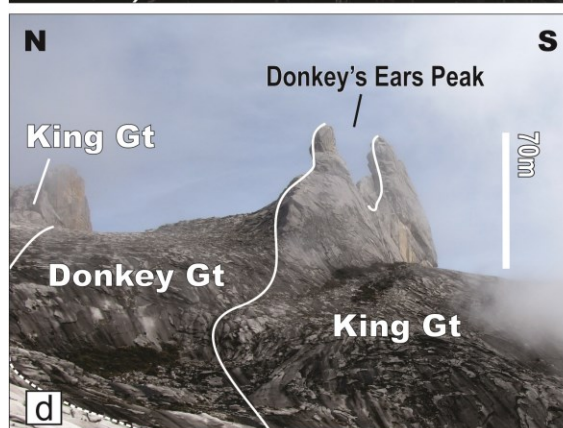
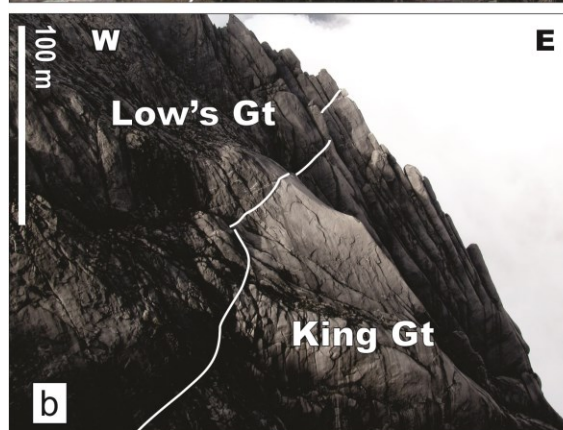
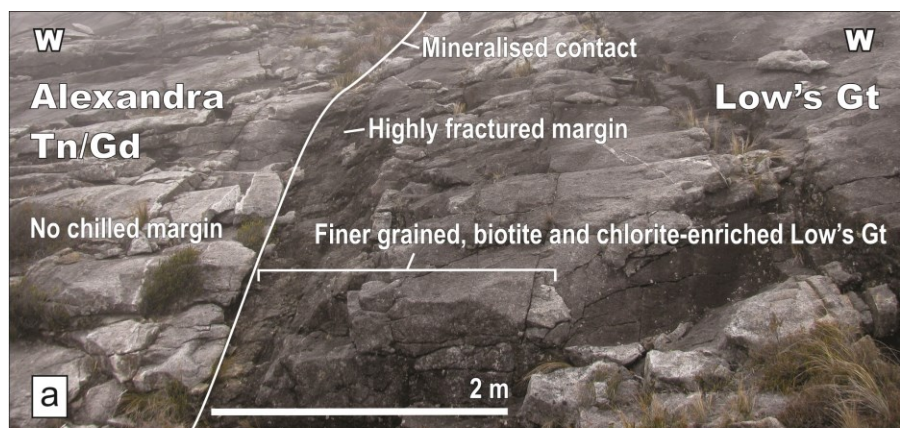


743

744

745 Fig. 9. View of the Western Plateau looking east, showing the contact between the
 746 Alexandra Tonalite/Granodiorite (Alexandra Tn/Gd, foreground) and the Low's Granite
 747 (Low's Gt). Field of view ~1.3km;

748

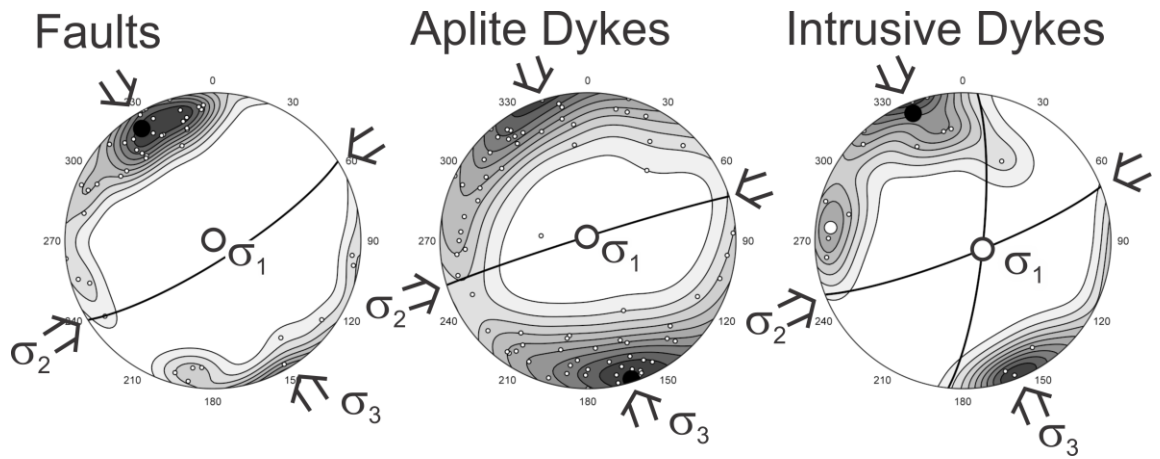


749

750

751 Fig. 10. (a) Contact of the Alexandra Tonalite/Granodiorite (Alexandra Tn/Gd) and the
752 Low's Granite (Low's Gt) on the Western Plateau, west of Victoria Peak (Fig. 5). Photo
753 looking north; (b) Contact of the Low's Granite and King Granite (King Gt) units on the
754 eastern cliffs of the Western Plateau. Photo looking north. Field of view ~300 m; (c)
755 Looking east towards Low's Gully from the Donkey Granite outcrops of the Western
756 Plateau, north of the Donkey's Ears (Fig. 5); (d) Contact of the Donkey Granite (Donkey
757 Gt) within the King Granite on the Western Plateau showing the resulting topographic
758 feature of the Donkey's Ears Peak. Photo looking NE from the summit trail; (e) Magma
759 mingling between The Donkey Granite (dark grey unit) and the King Granite (light grey
760 unit) on the NW contact on the Western Plateau. Photo looking south. Sledgehammer
761 for scale; (f) Contact of the King Granite and Paka Porphyritic Granite (Paka Pph) on the
762 southern flanks of Mt Kinabalu where the contact dips steeply south beneath the Paka
763 Porphyritic Granite. Photo looking west; (g) Contact between the King Granite and Paka
764 Porphyritic Granite on the east of the Eastern Plateau showing the Paka Porphyritic
765 Granite dipping beneath the King Granite. Photo looking north. (h) Pyroxene monzonite
766 (Pyx Mon) dykes intruding the Alexandra Tonalite Granodiorite on the north end of the
767 Western Plateau, showing their preferential erosion and vegetation. Photo looking west.
768 Note: Photographs taken in 2011, prior to the damage to the Donkey's Ears Peak during
769 the earthquake of 2015.

770

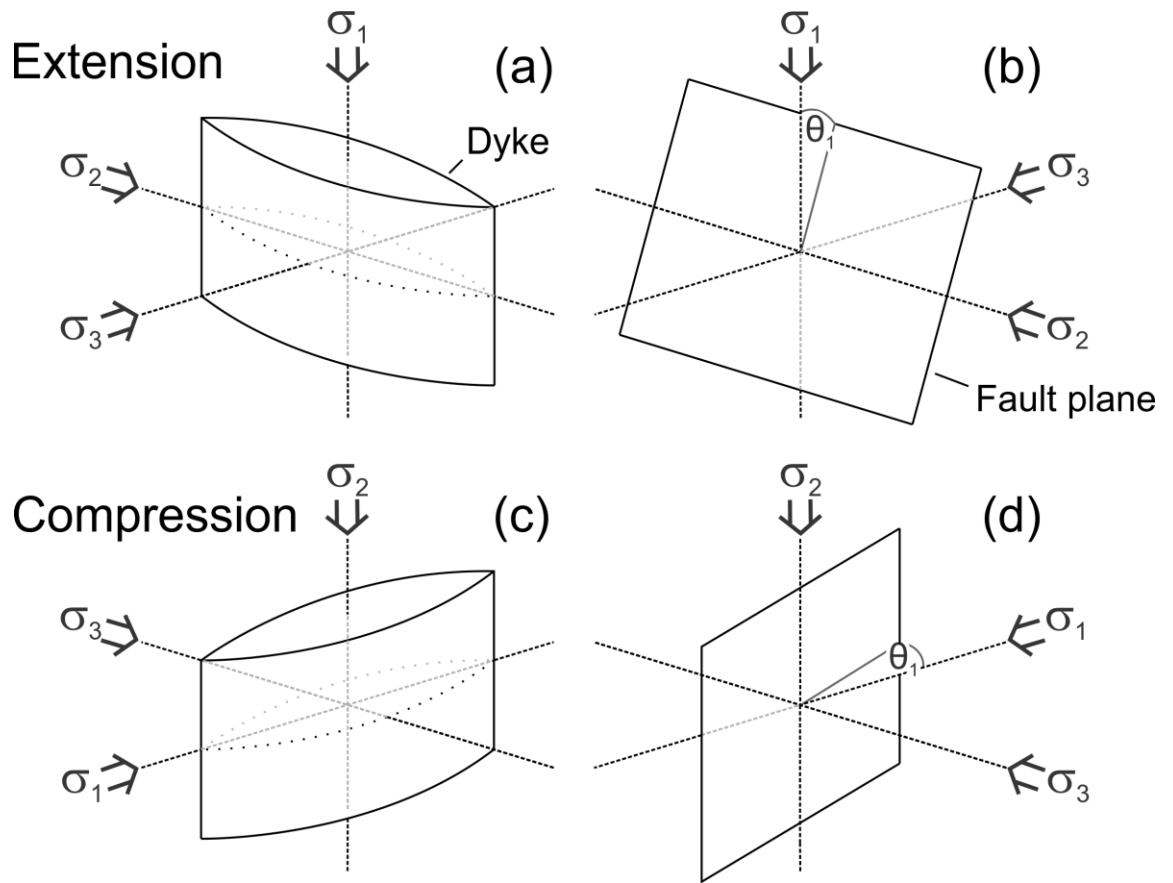


771

772

773 Fig. 11. Stereonets of poles to planes for fault ($n = 46$), aplite dyke ($n = 77$) and intrusive
 774 dyke ($n = 15$) orientations on Mt Kinabalu with probability density contours at 10% intervals
 775 (Vollmer 2015). The maximum eigenvectors and their great circles are shown (black circles
 776 and thick black lines), as are the interpreted principal stress directions. The intrusive dyke
 777 orientations are bimodal and the maximum eigenvectors are shown for each domain
 778 (black and white circles with corresponding great circles).

779



780

781

782 Fig. 12. Illustrations of the relationships between planar dyke (a and c) and fault (b and
 783 d) orientations relative to the principal stress axes in compressional and extensional
 784 regimes. σ_1 – Maximum compressive stress; σ_2 – Intermediate compressive stress; σ_3 –
 785 Minimum compressive stress; θ_1 – Angle between the fault plane and the σ_1 axis.